Modeling Earth Systems and Environment (2026) 12:113
https://doi.org/10.1007/s40808-026-02747-2

ORIGINAL ARTICLE

Rheology of melting and heat transfer progress of gallium in heterogeneous chamber containing metal foam and nanoparticles under influence of magnetic field

Atef Chibani[1] · Slimane Merouani[2] · Riad Badji[1] · Farhan Lafta Rashid[3] · Mohamed R. Eid[4] · Basma Souayeh[5] · Ibrahim Mahariq[6,7,8,9] · Mohamed Kezzar[10] · Mohamed Rafik Sari[11]

Received: 11 August 2025 / Accepted: 10 February 2026 / Published online: 17 March 2026

Abstract

In this work, melting characteristics and heat transfer enhancement of gallium as phase change material (PCM) surrounded by heterogeneous chamber filled with metal foam and Al_2O_3 nanoparticles under magnetic field are investigated. The main challenge rather is the low thermal conductivity of PCMs which in turn limits the performance of PCM based TESSs. Numerical simulations were performed using a 2D transient model developed by employing the enthalpy-porosity model and Darcy–Brinkman equations for the porous domain; where one of the boundary walls was kept at a heated temperature of 43 °C. It is found that the incorporation of metallic foam and nanoparticles greatly enhances both thermal conductivity and facilitates uniform melt. In addition, the magnetic field promotes such convective heat transfer, speeds up the melting rate, and raises the mean Nusselt number and surface heat flux. These results indicate that the integration of metal foams and nano/micro particles, and magnetic fields could be used to maximize the thermal performance of PCMs, which can lead to advanced TES applications with a high potential.

Keywords Heat transfer enhancement · Phase change materials · metal foam · nanoparticles · magnetic field · Melting behaviour

✉ Ibrahim Mahariq
ibmahariq@gmail.com

✉ Mohamed Kezzar
m.kezzar@univ-skikda.dz

Atef Chibani
chibaniatef@gmail.com

Slimane Merouani
s.merouani@yahoo.fr

Riad Badji
r.badji@crti.dz

Farhan Lafta Rashid
farhan.lefta@uokerbala.edu.iq

Mohamed R. Eid
mohamed.eid@nbu.edu.sa

Basma Souayeh
bsouayeh@kfu.edu.sa

Mohamed Rafik Sari
mohamed-rafik.sari@univ-annaba.dz

1 Research Center in Industrial Technologies CRTI, Cheraga, Algiers, Algeria

2 University Salah Boubnider-Constantine 3, Constantine, Algeria

3 University of Kerbala, Karbala, Iraq

4 Northern Border University, Arar, Saudi Arabia

5 King Faisal University, Al-Ahsa, Saudi Arabia

6 College of Engineering and Architecture, Gulf University for Science and Technology, Mishref, Kuwait

7 Najjad Zeenni Faculty of Engineering, Al-Quds University, Jerusalem, Palestine , Jerusalem, Palestine

8 Department of Electrical and Electronic Engineering, Faculty of Engineering and Architecture, Istanbul Gelisim University, Avcılar, Istanbul 34310, Istanbul, Turkey

9 University College, Korea University, Seoul 02481, South Korea, Korea

10 Materials and Energy Engineering Laboratory (LMGE), Technology Department, Faculty of Technology, 20 Aout 1955 University of Skikda, PO Box 26, 21000, , Skikda, Algeria

11 Mechanics of Materials and Plant Maintenance Research Laboratory (LR3MI), Faculty of Technology, Badji Mokhtar-Annaba University, P.O. Box 12, Annaba, 23000, Algeria., Annaba, Algeria

Introduction

Scholarly interest in nanofluids, which are colloidal solutions made up of particles with sizes ranging from the nanometer to the millimeter scale, has significantly increased in recent years. These materials' exceptional thermal and physical properties might be advantageous in several domains, such as energy conversion systems, biomedical engineering, and electronics cooling. The nanomolecules high surface-to-volume ratio and efficient convection and radiation heat transmission are responsible for the usual behavior that has been observed. A base fluid's behavior becomes nonlinear when nanoparticles are added due to changes to its rheological and transport properties (Prasad et al. 2024; Khan et al. 2021; Andersson et al. 1992). Researchers have recently been interested in energy storing utilizing phase change materials (PCMs) because of its many uses in electronic cooling, heat exchangers, solar power, thermal managing in various heat transference (HT) strategies, and building energy. The efficacy of PCM in various energy systems has been improved by a diversity of methodologies, including the use of metal foams, conductive fins, nanoparticles, and many more (Seeniraj and Lakshmi Narasimhan 2008; Hosseinizadeh et al. 2011; Ghalambaz et al. 2017; Rostami et al. 2020; Selimefendigil et al. 2022). Sadly, the poor thermal conductance of PCM used in energy storing devices lowers the rate of heat absorption (Li et al. 2020; Nóbrega et al. 2020; Khademi et al. 2022). The use of nanoparticles may improve the thermal conductance of a PCM, even for a tiny fractional size of nanomolecules, according to several ways that have been presented to enhance the thermal efficacy of the storage items. The impact of nanoparticles on improving the thermo-physical and heat transference possible of common liquids has been thoroughly investigated (Wang et al. 2022; Leong et al. 2021).

Moghadassi et al. (2015) explored the influences of a 0.1% volume concentration of H_2O-based aluminum oxide and aluminum oxide single bond copper hybridized nanoliquid on laminar forced convecton heat transference are investigated numerically. Their findings showed that the hybridized nanoliquid had an extremely greater convection heat transference factor. Tilehnoee et al. (2020) analyzed free convective flowing with entropy generation using the finite volume approach. The geometry under discussion comprises a rectangular wavy heater block situated on the bottom of the hollow wall and a permeable enclosure in the shape of an incinerator that is filled with Al_2O_3–H_2O nanofluid. The following is a list of more noteworthy studies in the area of magneto thermal convective flowing in the existence of complicated geometry. Huang et al. (2015) showed a 3D computational examination on the unstable free convective flowing in a square cavity occupied with air and subjected to sinusoidal temperature on one sidewall; benchmark solutions are produced utilizing a temporal–spatial pseudo-spectral approach that is very accurate. They investigated how the amplitude, period, and Rayleigh number (between 10^3 and 10^6) of the pulsing sidewall temperature affected the liquid flowing patterns and heat transference capabilities within the cavity. Chorin et al. (2018) investigated numerically the heat transport in a two-dimensional cavity, a local thermal disturbance placed at a single location on the hot wall. The disturbance is in the space between height $Z_1 = 20$ and $Z_2 = 25$. Global heat transport is affected by the local change in two ways: around 2% on the opposing cold wall and roughly 16% downstream in the disturbance region.

Dahmani et al. (2022) developed an innovative design that uses ferrofluid and an external magnetized force produced by a current-carrying wire to improve heat transference in parabolic trough solar collector absorbers. The findings showed that a disrupted flowing with a high-speed area close to the current-carrying wire is produced by the occurrence of an uneven magnetized force. The optimization of nanofluid heat transfer performance is the primary emphasis of the aforementioned literature on non-uniform magnetic fields. The nonuniform magnetized forces have been intentionally used to enhance the NEPCMs' melting and solidification procedures. Shakiba and Vahedi (2016) examined the heat transference factor and pressure dropping in a twin-pipe heat exchanger with a ferrofluid in the inner tube and an external nonuniform magnetized force (created by a wire carrying current parallel to the tube). They noticed that a few vortices formed because of the magnetized force producing a Kelvin force perpendicular to the ferrofluid flowing. When compared to the situation without a magnetized force, this produced secondary flow caused the Nusselt number to rise by 45% (for $Re = 50$). The research also confirms that expanding the Reynolds numbers lessens the impact of the external magnetic field. Shatikian et al. (2005a) carried out numerical work for the melting of a PCM in a storage unit with aluminum internal fins. They used finite volume-based code and unstable 2D/3D simulations to conduct a thorough parametric investigation for various fin characteristics and PCM thickness. They observed that the Fourier and Stefan numbers influenced the Nusselt number (Nu) and melted percentage. The impacts of convection at mature stages should be considered for vast vertical PCMs.

However, the low thermal conductivities of PCMs remain a major obstacle to efficient heat transfer (Li et al. 2020). To elaborate this, conductive structures such as metallic foams (Li et al. 2020) and the addition of nanoparticles (Ghalambaz et al. 2017; Rostami et al. 2020) have been proposed to enhance thermal performance. Furthermore, recent studies have shown that irregular magnetic fields can improve heat transfer in nanofluids (Shakiba and Vahedi 2016) and in PCM systems (Selimefendigil et al. 2022). Nevertheless, most published research has focused on improving heat transfer using one of these technologies (foam, nanoparticles, or a magnetic field) separately, or by combining only two of them. For example, Ref. (Li et al. 2020) focused on the effect of metallic foam alone, while Ref. (Dahmani et al. 2022) investigated the effect of a magnetic field on nanofluids without including PCM or metallic foam. Ref. (Shakiba and Vahedi 2016) tested the effect of a magnetic field on the performance of a heat exchanger using a nanofluid without considering phase transition or the porous environment. Therefore, a clear research gap exists in investigating the combined and interactive effect of these three components (metal foam + nanoparticles + magnetic field) on PCM melting behavior and heat transfer improvement. This research addresses this gap by achieving the following:

- Three optimization mechanisms were integrated into a single model: a metallic foam (to improve conductivity), nanoparticles (to enhance thermal properties), and a magnetic field (to improve heat transfer).
- The effect of magnetic flux density on the melting rate and heat distribution in a PCM-foam-nano system was investigated, a topic not explored in Li et al. (2020); Dahmani et al. 2022; Shakiba and Vahedi 2016).
- The quantification of heat transfer optimization was achieved by calculating the fluid fracture evolution, average Nusselt number, and total enthalpy under different magnetic conditions.

This work makes a numerical study of the joint action of metal foam and nanoparticles in a PCM-filled chamber under magnetic field to improve heat transfer and melting rate. A two-dimensional transient model including a tangential enthalpy method for the phase change was developed by means of ANSYS Fluent software. Using the Darcy–Brinkman model of porous metallic foam, the work investigated the influences of magnetic flux density on temperature distributions, liquid fraction evolution, Nusselt numbers and heat flow by a parametric study. The fact this paper is novel enough to explore the use of the loading rate of phase change materials (PCMs) and thermal conductance development of PCMs in a heterogeneous chamber containing metal foam and nanoparticles, the field which has not been studied enough as the system of thermal energy storage. This research aims to assess the impact of these improved materials on thermal conduction and the heat transfer rate of PCMs with a heated wall at 43°C. Through computational modeling of the temperature fields and velocities during phase transformation, this research seeks to establish information on the fluid behavior and thermal characteristics of PCMs as useful in formulating enhanced thermal energy storage systems. With this knowledge, the paper aims to highlight potential areas of research for the development of novel approaches in energy control and advanced thermal performance technologies of buildings.

Simulation and mathematical model

Governing equations for PCM

This research incorporates the standard assumptions of transient formulation and two-dimensional Newtonian incompressible fluid, accounting for natural convective influences. Although they could vary for the liquid and solid phases, the PCM's thermophysical characteristics are thought to remain constant. Variations in liquid density only occur in the buoyancy source term and are otherwise ignored, according to the Boussinesq approximation (Keshteli and Sheikholeslami 2020; Bouzennada et al. 2020), which is valid. The conservation rules must be represented in their corresponding integral forms since the current formulation deals with solutions to unstructured grids. Given the aforementioned presumptions, the continuity, momentum, and energy conservation equations may be expressed as (Ji et al. 2018; Gorzin et al. 2019):

Mass conservation

$$\vec{\nabla}.\vec{V} = 0. \tag{1}$$

Momentum conservation

$$\rho_{pcm}\left[\frac{\partial\vec{V}}{\partial t} + \left(\vec{V}\vec{\nabla}.\vec{V}\right)\right] = -\nabla\vec{P} + \nabla\left(\mu.\nabla.\vec{V}\right) - \rho_{pcm}\vec{g}\left(1-\beta.\left(T-T_m\right)\right) - \sigma_f B_0^2\vec{V} + A\vec{V}, \tag{2}$$

$$A = -A_{mush}\frac{\left(1-f_l\right)^2}{f_l^3 + 0.001}, \tag{3}$$

Energy equations

$$\rho\frac{\partial h_{sens}(T)}{\partial t} + \nabla.h_{sens}(T)\,\rho\vec{V} = \nabla\left(\lambda.\nabla T\right) - \rho\left(\frac{dh_{lat}}{dt} + \vec{V}.\vec{\nabla}.h_{lat}\right), \tag{4}$$

where $h_{sens}(T)$ denotes the sensible heat associated with the energy accumulated due to the temperature increase of the solid or liquid substance, as articulated in Eq. (4) (Kok 2020):

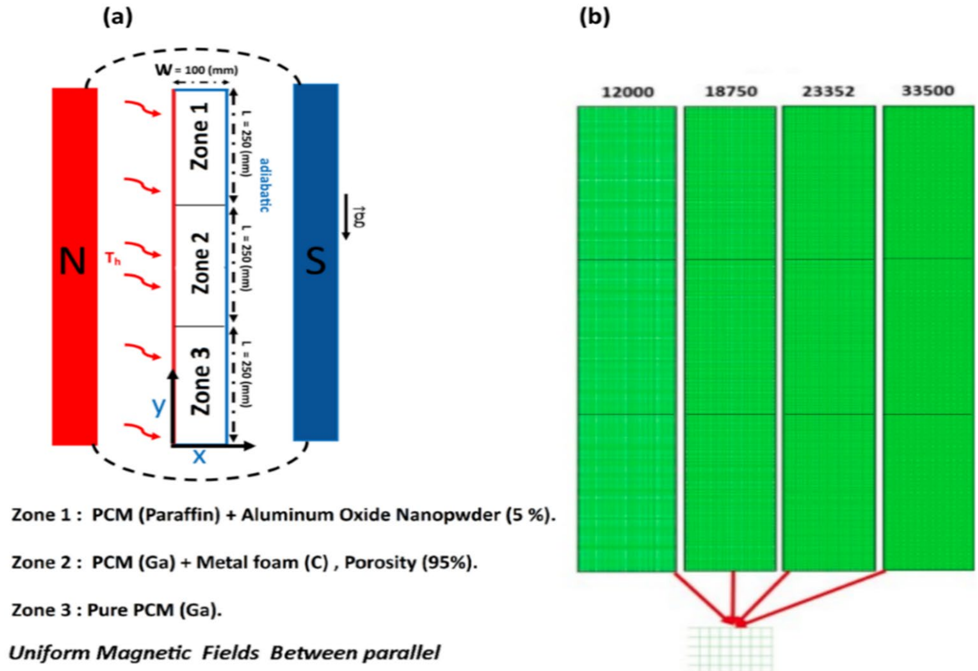

Fig. 1 (**a**) Diagrammatic illustration of the filled heat storage chamber and (**b**) Computational grids for the system studied

$$h_{sens}(T) = h_{ref} + \int_{Tref}^{T} C_p dT, \tag{5}$$

where h_{ref} represents the reference enthalpy at the reference temperature ($T_{ref} = T_m = 302.93K$) and C_p signifies the specific heat a. a fixed pressure. The energy absorbed by a substance throughout its phase transition is denoted by the latent energy component $h_{lat}(T)$ in Eq. (5), which may be articulated using the following formula (Kok 2020):

$$h_{lat}(T) = f(T).\Delta h_{s-l}, \tag{6}$$

Equation (7) is employed to corre.a.e sensible heat and fluid fraction, including iterations between the energy formula and the fluid fraction formula.

$$f = \begin{cases} 0, T \le T_S, \\ \frac{T-T_s}{T_l-T_s}, T_s \le T \le T_l, \\ 1, T \ge T_l, \end{cases} \tag{7}$$

where s and l are indexes for the solid and liquid phases of phase change materials (PCM). The Boussinesq approximation is used here, where density changes are considered only at the buoyancy term, while the fluid is treated as incompressible. This approximation is suitable for small temperature changes as well as average density changes. This is used in many studies related to the melting of phase-change materials (Bouzennada et al. 2020; Ji et al. 2018). When MHD impact is present, this approximation remains valid as long as the magnetic field does not cause significant Joule heating or, in turn, produce significant compressive effects. This constraint occurs when the magnetic Reynolds numbers ($Re_m \ll 1$) decrease and the moderate magnetic flux densities ($B_0 \le 0.001T$) adopted in this study.

Foam layer (porous medium/PCM-MF)

The continuity and momentum formulas in a porous and transparent zone are part of the hydraulic equations that control fluid flow. The Darcy-Brinkman prototype manages to construct the momentum equation in the porous zone. The following are the momentum equation in the clear area and the continuity equation in the porous region (Golbaghi Masouleh et al. 2022; Lu et al. 2006; Vafai and Tien 1981):

Continuity equation:

$$\frac{\partial \rho}{\partial t} + \rho\left(\frac{\partial u}{\partial x} + \frac{\partial v}{\partial y}\right) = 0, \tag{8}$$

Momentum equation in x− direction

$$\frac{\rho}{\varepsilon}\frac{\partial u}{\partial t} + \frac{\rho}{\varepsilon^2}\left(u\frac{\partial u}{\partial x} + v\frac{\partial v}{\partial y}\right) = \frac{\mu}{\varepsilon}\left(\frac{\partial^2 u}{\partial x^2} + \frac{\partial^2 v}{\partial y^2}\right) - \frac{\partial P}{\partial x} - \left(\frac{\mu}{K}u + \frac{C_i}{\sqrt{K}}u\sqrt{u^2+v^2}\right) + S(u), \tag{9}$$

The magnetic force per unit volume ($\overrightarrow{F}_m$) comes from the Lorentz force acting on an electrically conducting fluid in a static magnetic field. When the Reynolds number ($Re_m \ll 1$) is small, then the induced magnetic field is small compared to the applied field $\overrightarrow{B}$. The general form is:

Table 1 Main thermal-physical attributes of the worked

Parameter	Value
(Pure gallium) (Chibani et al. 2024; Zennouhi et al. 2017; Çolak et al. 2022)	
Thermal conductance (W/mK)	32
Specific heat (J/kgK)	381.5
Latent heat of fusion (J/kg)	80,160
Melting temperature T_m (K)	302.93
Reference temperature T_{ref} (K)	302.93
Density (kg/m^3)	6093
Viscosity (kg/m.s)	$1.81 \cdot 10^{-3}$
Electrical conductivity (σ_f) (S/m)	3.9×10^6
Magnetic field strengths (B_0) (T)	0, 0.001, 0.01, 0.1
Volumetric thermal expansion coefficient of liquid (K^{-1})	1.2×10^{-4}
Reference density (kg/m^3)	6095
Paraffin (RT25HC) (Kıyak et al. 2024; Öztop et al. 2024)	
Thermal conductivity (W/mK)	0.19
Specific heat (J/kgK)	1800
Latent heat of fusion (J/kg)	230,000
Melting temperature T_m (K)	298.15
Reference temperature T_{ref} (K)	298.15
Density (kg/m^3)	880 (solid) 770 (liquid)
Viscosity (kg/ms)	0.026
Volumetric thermal expansion coefficient of liquid (K^{-1})	0.0006
Reference density (kg/m^3)	770
Graphite (Chibani et al. 2022, 2023b)	
density (kg/m^3)	2,266
specific heat (J/kgK)	170
Thermal conductivity (Wm^{-1}K^{-1})	720
Aluminum Oxide Al_2O_3 (Keshteli and Sheikholeslami 2020; Saha 2020)	
density (kg/m^3)	3970
specific heat (J/kgK)	170
Thermal conductivity (Wm^{-1}K^{-1})	25
Volumetric thermal expansion coefficient of liquid (K^{-1})	1.2 10^{-4}
Diameter of nanoparticle (μm)	47
Electrical conductivity (Ω^{-1}m^{-1})	1×10^{-10}

$$\vec{F}_m = \vec{J} \times \vec{B},$$

wherein $\vec{J} = \sigma\left(\vec{E} + \vec{V} \times \vec{B}\right)$ signifies the current density, when the fluid is static and there is no external electrical field $\left(\vec{E} = 0\right)$, this can be simplified to:

$$\vec{F}_m = \sigma\left(\vec{V} \times \vec{B}\right) \times \vec{B}.$$

For the magnetic field that applied only in the $y-$ direction ($\vec{B} = (0, B_0, 0)$), and velocity $\vec{V} = (u, v)$, the force components become $F_{mx} = 0$, $F_{my} = -\sigma_f B_0^2 v$ (Lorentz force in $y-$ direction), where σ_f indicates the electrical conductivity of the fluid.

$\boldsymbol{y}-$direction momentum equation includes the effects of magnetic, gravity, porosity, and concentration forces.

$$\frac{\rho}{\varepsilon}\frac{\partial v}{\partial t} + \frac{\rho}{\varepsilon^2}\left(u\frac{\partial v}{\partial x} + v\frac{\partial v}{\partial y}\right) = \frac{\mu}{\varepsilon}\left(\frac{\partial^2 v}{\partial x^2} + \frac{\partial^2 v}{\partial y^2}\right) - \frac{\partial P}{\partial y} - \left(\frac{\mu}{K}v + \frac{C_i}{\sqrt{K}}v\sqrt{u^2+v^2}\right) + \rho g\gamma\left(T - T_0\right) - \sigma_f B_0^2 v + S\left(v\right), \tag{10}$$

Energy equation:

$$\left[\varepsilon\rho_f C_{P,f} + (1-\varepsilon)\rho_s C_{P,s}\right]\frac{\partial T}{\partial t} + \varepsilon\rho_f C_{P,f}\left(u\frac{\partial T_f}{\partial x} + v\frac{\partial T_f}{\partial x}\right) = k_{eff}\left(\frac{\partial^2 T_f}{\partial x^2} + \frac{\partial^2 T_f}{\partial y^2}\right) + \varepsilon\rho_f L\frac{\partial \beta}{\partial t}, \tag{11}$$

The effective thermal conductance is calculated by

The effective thermal conductivity k_{eff} of the CPCM may be calculated using several techniques that are often used in the literature (Tian and Zhao 2011; Feng et al. 2015; Hu and Patnaik 2014). The following equation (Mesalhy et al. 2005) is used to determine Keffin Eq. (12):

$$k_{eff} = \frac{\left[k_s + \pi\left(\sqrt{\frac{1-\varepsilon}{3\pi}} - \frac{1-\varepsilon}{3\pi}\right)(k_f - k_s)\right]\left[k_s + \frac{1-\varepsilon}{3}(k_f - k_s)\right]}{k_s + \left[\frac{4}{3}\left(\sqrt{\frac{1-\varepsilon}{3\pi}}(1-\varepsilon)\right) + \pi\sqrt{\frac{1-\varepsilon}{3\pi}} - (1-\varepsilon)\right](k_f - k_s)}, \tag{12}$$

The solid matrix, the applicable characteristics of the suspension and porous material, and the bulk characteristics of the suspension are denoted by the subscripts s, m, and b, respectively. Tadrist et al. (2004) used the empirical formula to determine the correlations between permeability (K) and the Forchheimer coefficient (C_i).

$$K = \frac{\varepsilon^2 d_f^2}{100(1-\varepsilon)^2}, \tag{13}$$

$$C_i = \frac{0.65(1-\varepsilon)}{\varepsilon^2 d_f}, \tag{14}$$

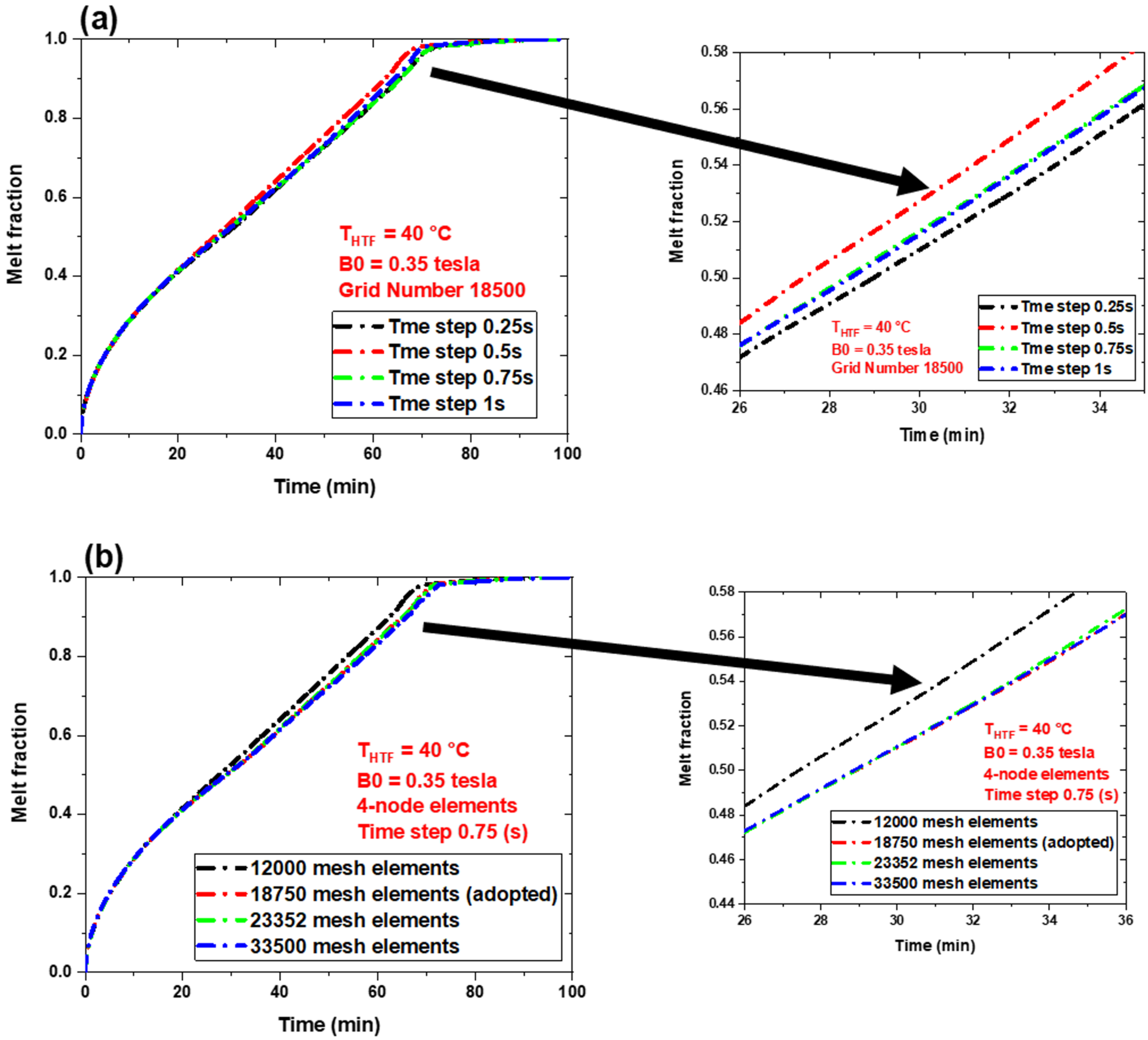

Fig. 2 (**a**) Time step and (**b**) Grid independence verification based on melt fraction results

where d_f and ε are the metal foam's strut diameter and porosity. The present research makes use of copper foam. According to Kumar et al. (2014), the foam's porosity is 0.9 and the strut diameter is 0.534 mm.

$$S = \frac{C(1-\beta^2)}{\alpha+\beta^3}, \tag{15}$$

$$\beta = \frac{\Delta H_{pcm}}{L_{pcm}} = \begin{cases} 0, T \le T_S, \\ \frac{T-T_s}{T_l-T_s}, T_s \le T \le T_l, \\ 1, T \ge T_l, \end{cases} \tag{16}$$

where s and l are indexes for the solid and liquid phases of phase change materials (PCM).

In relationship of latent heat of fusion L_{pcm}, ΔH_{pcm} is the fractional latent heat of the PCM that increases throughout the phase change management.

$$\Delta H_{pcm} = \begin{cases} 0 if T < T_m \\ \beta.L_{pcm} if T > T_m \end{cases} \tag{17}$$

The summation of sensible and latent heat, or the PCM's total enthalpy H, is as follows:

$$H = h + \Delta H_{pcm}, \tag{18}$$

The sensible enthalpy, denoted by h, is expressed as follows:

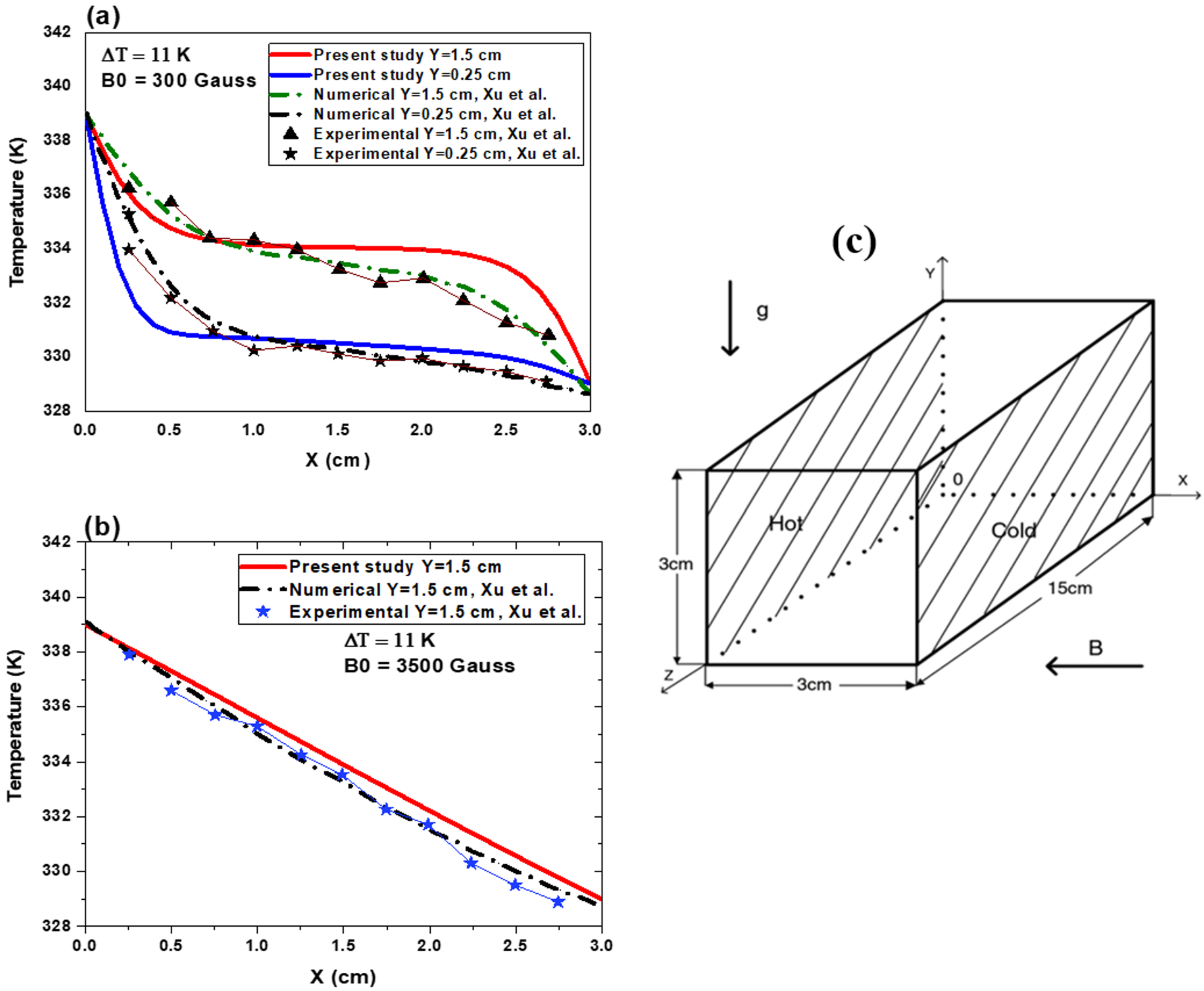

Fig. 3 Verification temperature of the current result obtained by Xu et al. (Chibani et al. 2024)

$$h = h_{ref} + \int_{T_m}^{T} \rho_{pcm} C_{p_{pcm}} dT, \tag{19}$$

Nanofluid properties

The characteristics of nano-PCM are altered when nanoparticles are present. With the exception of thermal conductivity, all of the effective characteristics of nano-PCM are constant and established utilizing the volume fraction of nanoparticles, which is computed as follows (Kant et al. 2020; Bechiri and Mansouri 2016; Khan et al. 2019):

$$\rho_{npcm} = (1 - \varnothing)\,\rho_{pcm} + \varnothing \rho_{np}, \tag{20}$$

$$C_{p_{npcm}} = \frac{(1 - \varnothing)\,\rho_{pcm} C p_{pcm} + \varnothing \rho_{np} C p_{np}}{\rho_{npcm}}, \tag{21}$$

$$L_{npcm} = \frac{(1 - \varnothing)\,\rho_{pcm} L_{pcm}}{\rho_{npcm}}, \tag{22}$$

$$\beta_{npcm} = \frac{(1 - \varnothing)\,\rho_{pcm} \beta_{pcm} + \varnothing \rho_{np} \beta_{np}}{\rho_{npcm}}, \tag{23}$$

The 1st half of this equation is derived from the Maxwell representation, whilst the 2nd half takes Brownian motion into account to explain why thermal conductivity temperature is dependent. This prototype considers the consequences of molecule size, operating circumstances, volume fraction, and thermo-physical characteristics for PCM and nanoparticles (Khan et al. 2019; Chibani et al. 2023a):

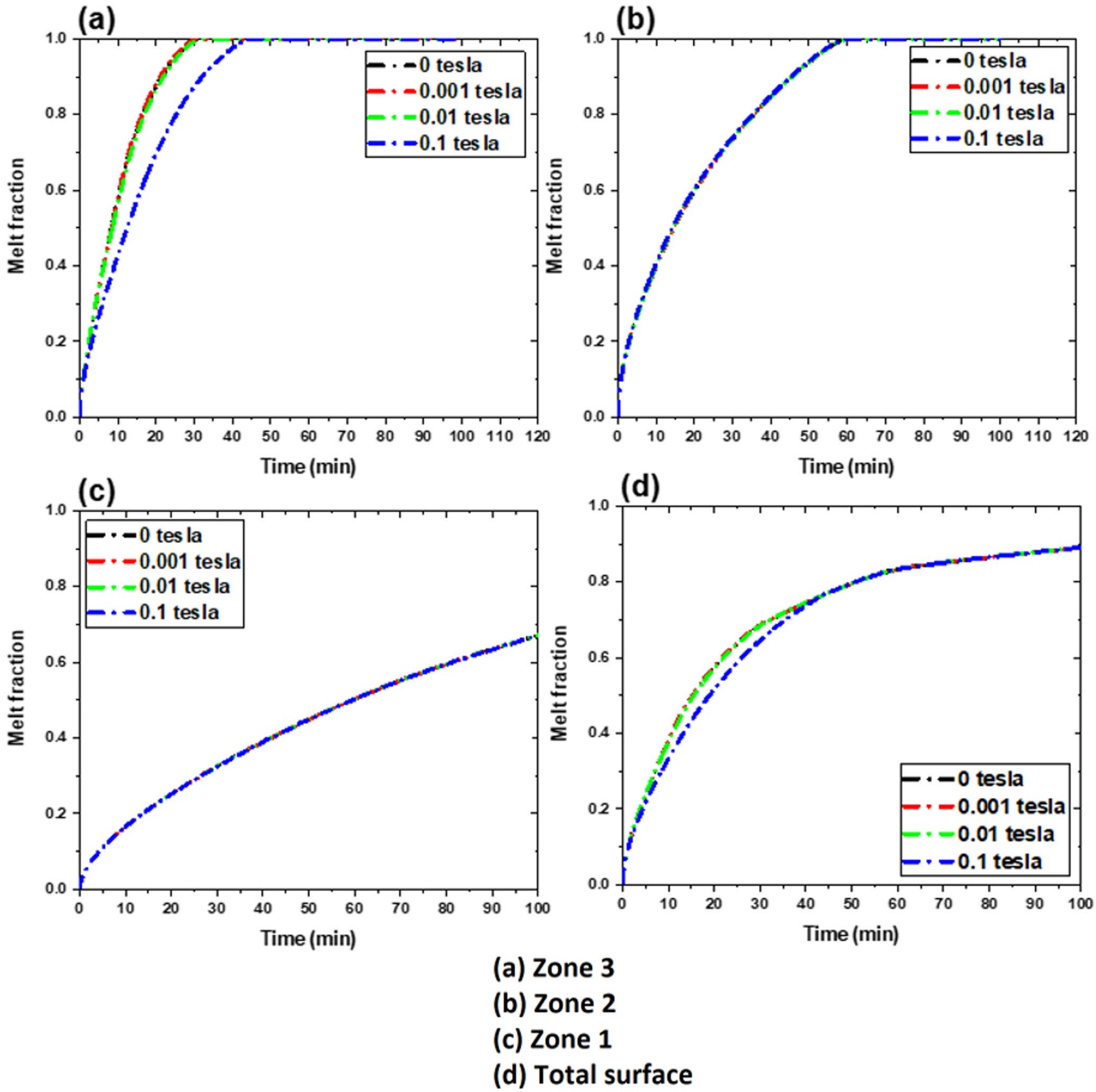

Fig. 4 Liquid fraction graph of PCM at diverse magnetic flux densities

$$k_{npcm} = \frac{k_{np} + 2k_{pcm} - 2\left(k_{pcm} - k_{np}\right)\emptyset}{k_{np} + 2k_{pcm} + \left(k_{pcm} - k_{np}\right)\emptyset} k_{pcm} + 5.10^4 \rho_{pcm} \emptyset c p_{pcm} \sqrt{\frac{K_B T_{pcm}}{\rho_{np} d_{np}}} f\left(T, \emptyset\right), \tag{25}$$

here the correction coefficient $f\left(T, \varnothing\right)$ is distinguished as:

$$f\left(T, \emptyset\right) = \left(2.8217 \times 10^{-2} \emptyset + 3.917 \times 10^{-3}\right) \frac{T_{npcm}}{T_{ref}} + \left(-3.0669 \times 10^{-2} \emptyset - 3.91123 \times 10^{-3}\right), \tag{26}$$

Using the representations of Vajjha et al. (2010), the effective dynamic viscosity of NePCMs containing Al_2O_3 nanoparticles is calculated:

$$\mu_{npcm} = 0.983 e^{(12.958.\varnothing)}.\mu_{pcm}, \tag{27}$$

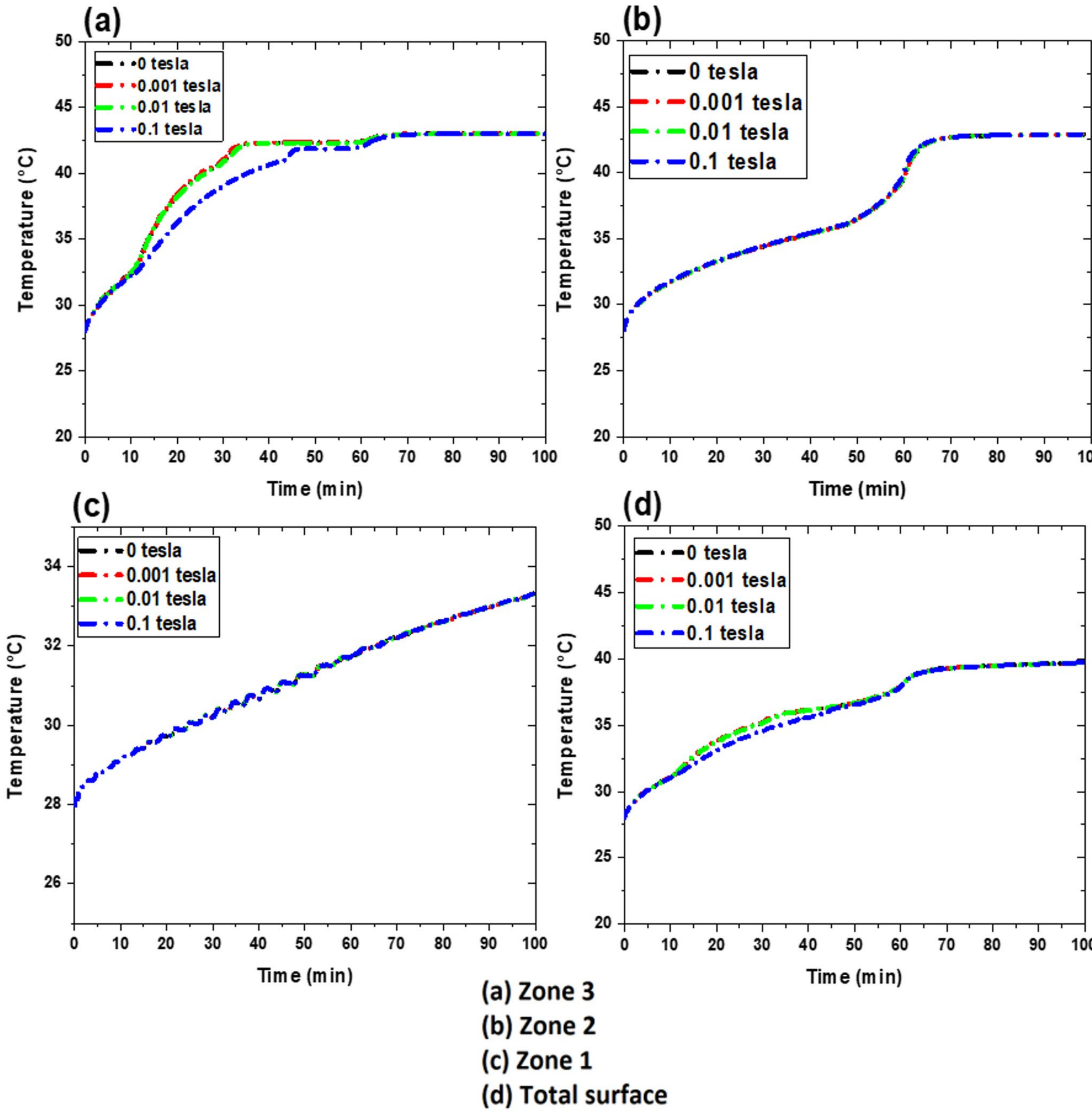

Fig. 5 Average temperature graph of PCM at diverse magnetic flux densities

Problem setup

The filled heat storing chamber is also illustrated in Fig. 1 part (a) of this paper while part (b) of the figure shows the computational grids used in the study. The heat storage chamber section discusses how thermal energy storage is used and how the PCM is incorporated into the system. The grids shown in part (b) represent the numerical simulation meshing technique used for the described fluid dynamics and heat transference in the chamber. This careful grid design is worthy in the overall precise measurement in the examination of the melting behavior and thermal characteristics of the PCM under different conditions.

Software that is sold commercially the regulating formulas are resolved in double-precision employing ANSYS-Fluent (Shatikian et al. 2005b). A 12th Gen Intel(R) Core (™) i5-12,400, 2.50 GHz processor is used for parallel computation. Phase change simulations are carried out using the enthalpy-porosity prototype created by Voller et al. (1987), and a pressure-based finite volume approach is used to

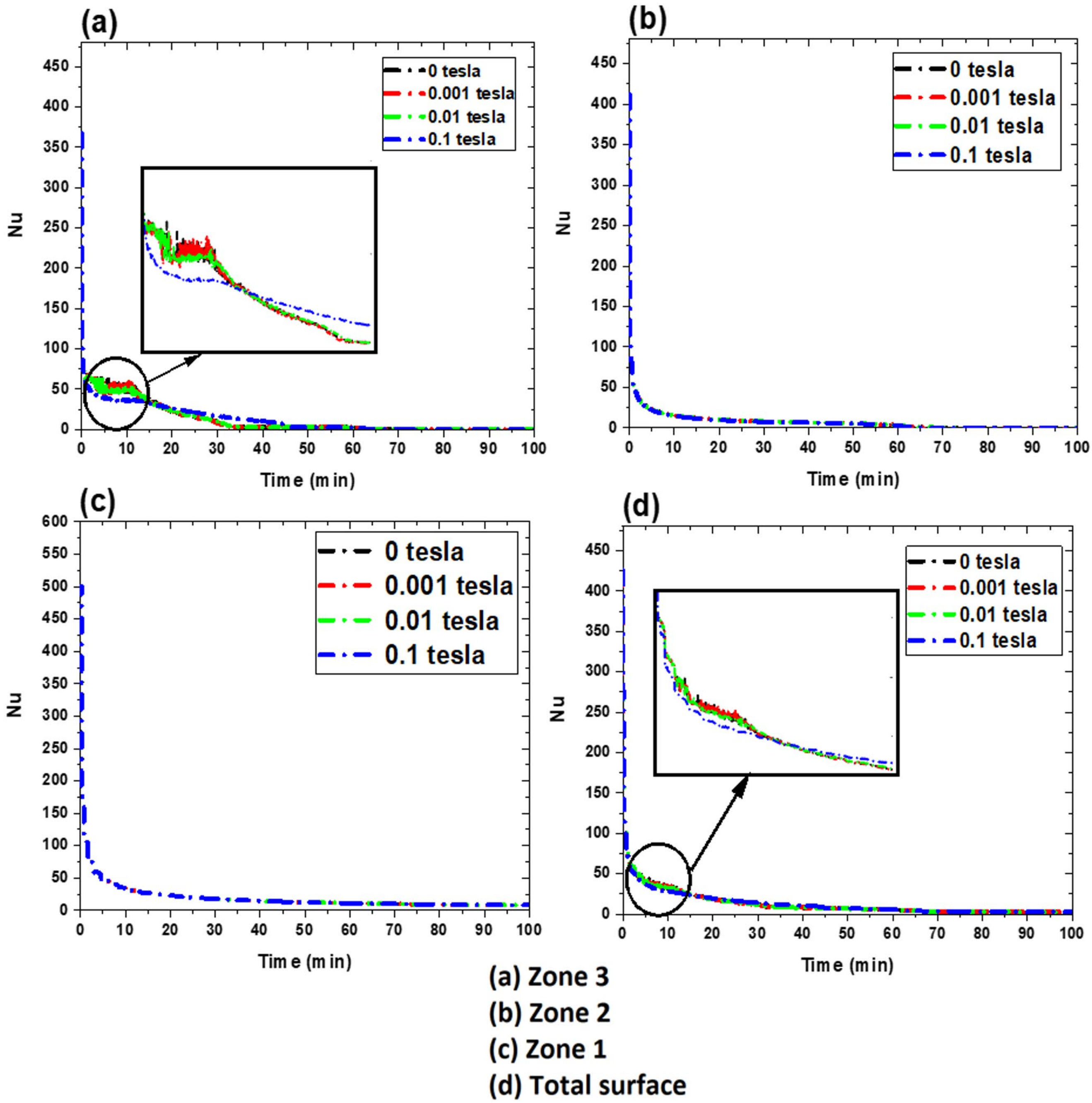

Fig. 6 Nu_{avg} graph of PCM at diverse magnetic flux densities

discretize the model's regulating formulas. A PISO method with a separated solver is exploited for the pressure–velocity coupling (Kang and Ryou 2004). Table 1 depicts the main thermal-physical attributes of the worked material value. The governing equations' convective components are discretized operating a 2nd-order upwind technique, and the PRESTO algorithm is employed to carry out the pressure–velocity coupling. For the continuity, momentum, and energy formulas, the residuals are set to 10^{-4}, 10^{-5}, and 10^{-9}, separately. Despite an elevated value of 200 iterations per time step, the real iterations required for convergence are far less. By running the same simulation with one distinct time step 0.75 s a time step sensitivity examination is carried out. These four distinct time step sizes are used to compare the liquid percentage of gallium at equivalent physical moments, and the difference between the findings is less than 1% shown in Fig. 2a To run the simulation, an unstructured mesh is created. Two grids are created to conduct a grid sensitivity/independence study. Two grids are prepared: a coarse grid with 12,000, 23,352, and 23,350 cells and a fine grid

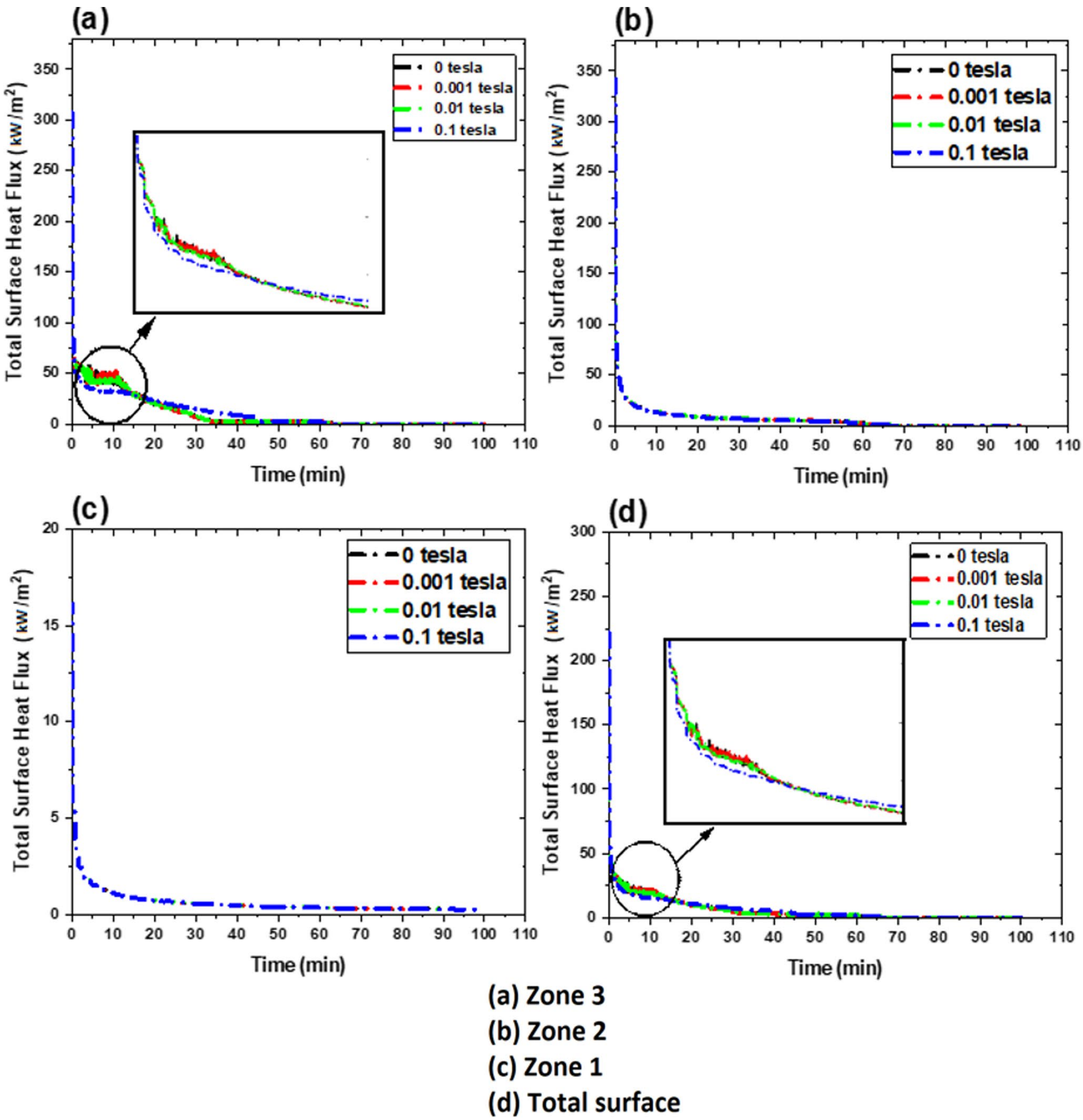

Fig. 7 Average total surface heat flux graph of PCM at diverse magnetic flux densities

with 33,500 cells, which is almost twice as many cells as the coarse grid. For both grids, the change in gallium (Ga)'s liquid percentage is displayed. The findings produced from the two grid sizes differed by less than 2%. This is because there were a lot of cells in both the coarse and fine grids. Additionally, the convergence criteria's residuals are maintained rigorously. Consequently, the combined impact of the two meshes produced very little variation in the outcomes. Figure 2b displays the results of the mesh sensitivity and time step assessments. The experiments shown in Fig. 2b are halted when the liquid fraction reached 100% since the findings demonstrated that the numerical calculations conducted are unrelated to grid size and time step.

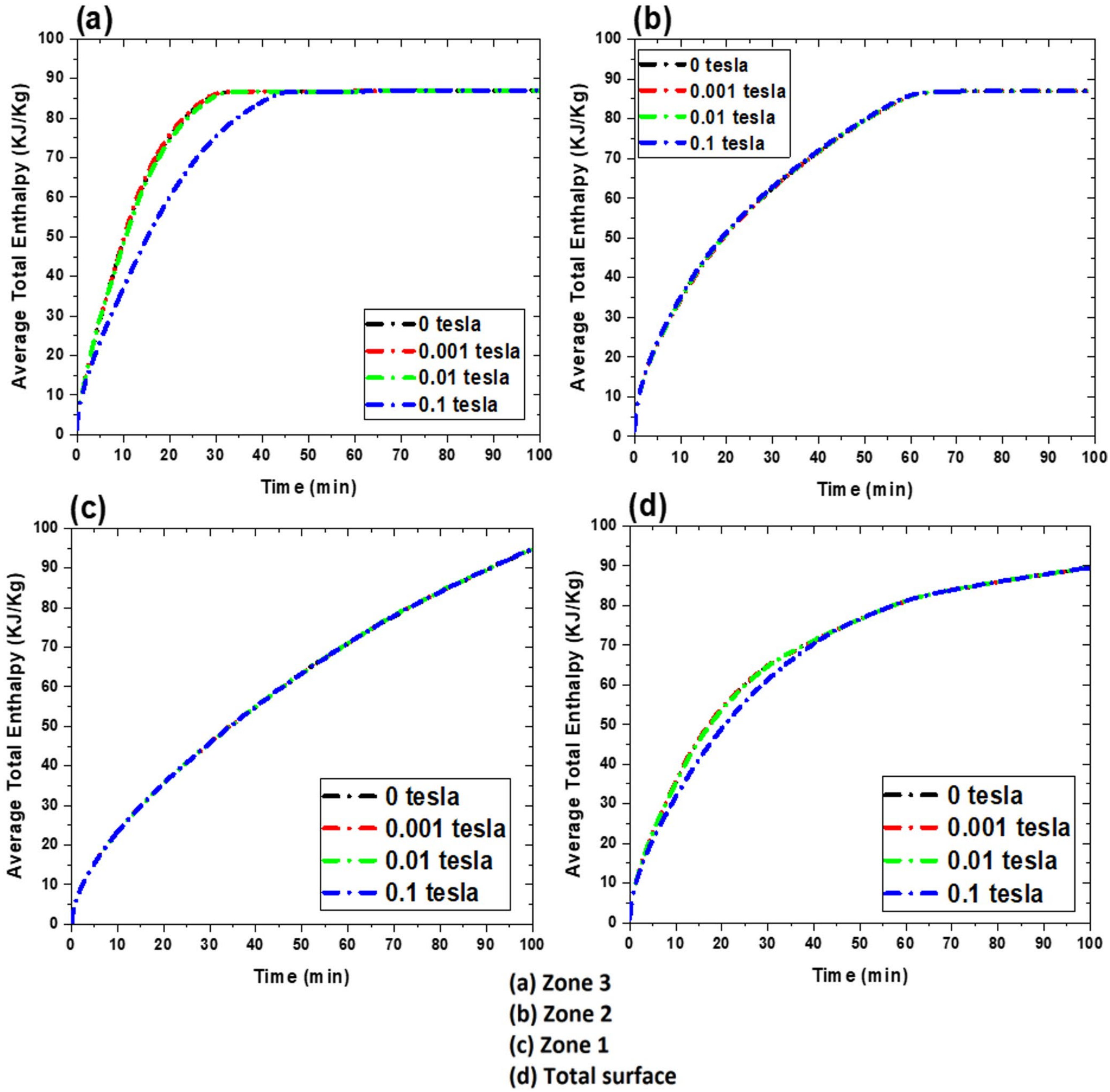

Fig. 8 Average total enthalpy graph of PCM at diverse magnetic flux densities

Results and discussion

As seen in Fig. 3, the verification of temperature results calculated in the current study yielded satisfactory results compared to the study by Xu et al. (Chibani et al. 2024). This temperature profile indicated the variations of temperatures at diverse locations (X) in the present numerical study with respect to the positions at certain vertical locations (Y) The marked point in the graph shows good accord between the present simulation outcomes and the empirical findings of Xu et al. (Chibani et al. 2024). The agreement of the calculated temperature in this regard with reference temperature as well as the agreement of the temperature values in

Table 2 Summarizing outcome data

Parameter	Pure PCM	PCM + MF + NPs	PCM + MF + NPs + B=0.001T
Melting time (up to 90%)	1100s	720s	520s
Nu_{avg}	12.3	21.5	28.9
Relative storage capacity (at 600 s)	1.0	1.48	1.72

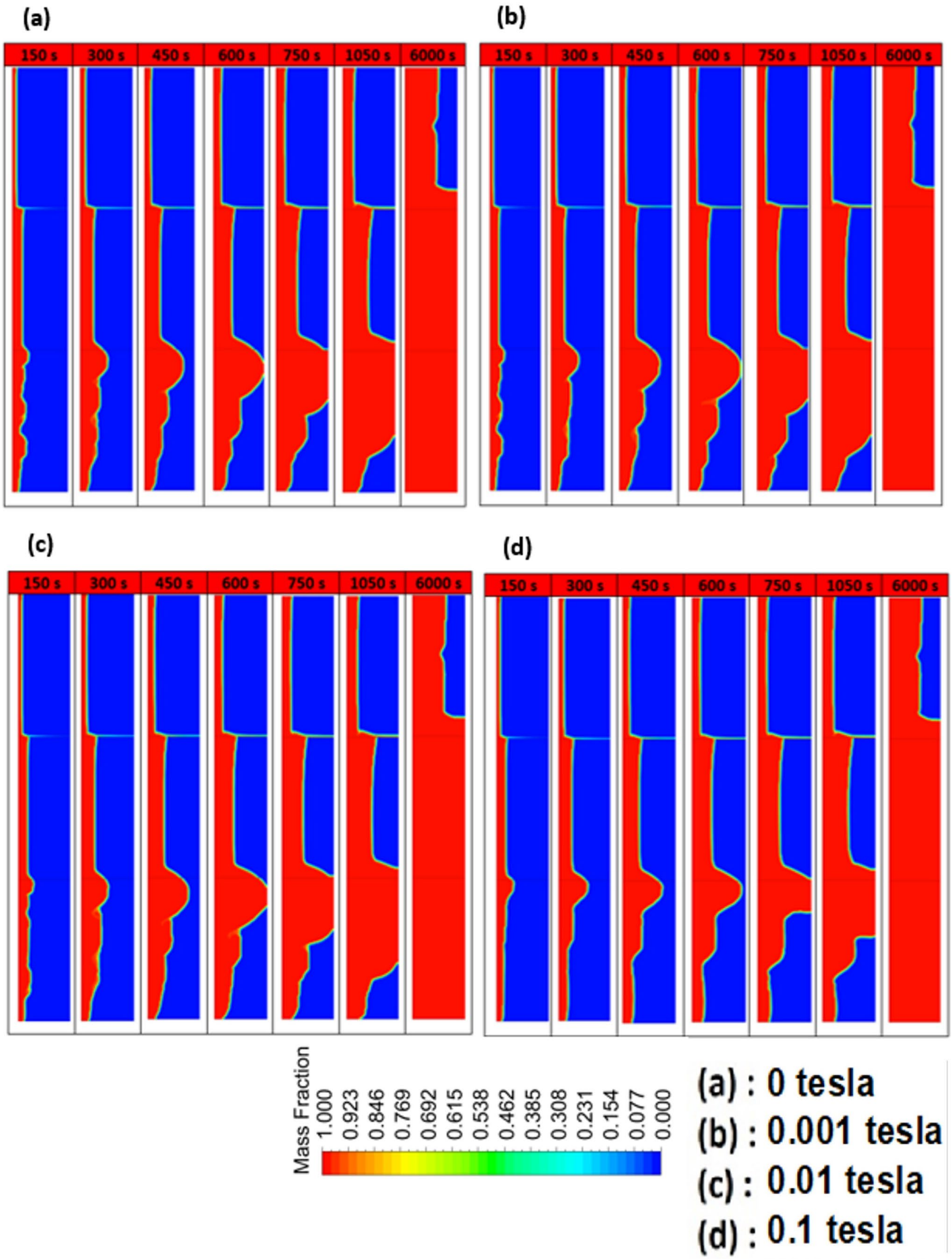

Fig. 9 PCM's transitions between the phases of solid and liquid during melting with a heated wall temperature of 43°C

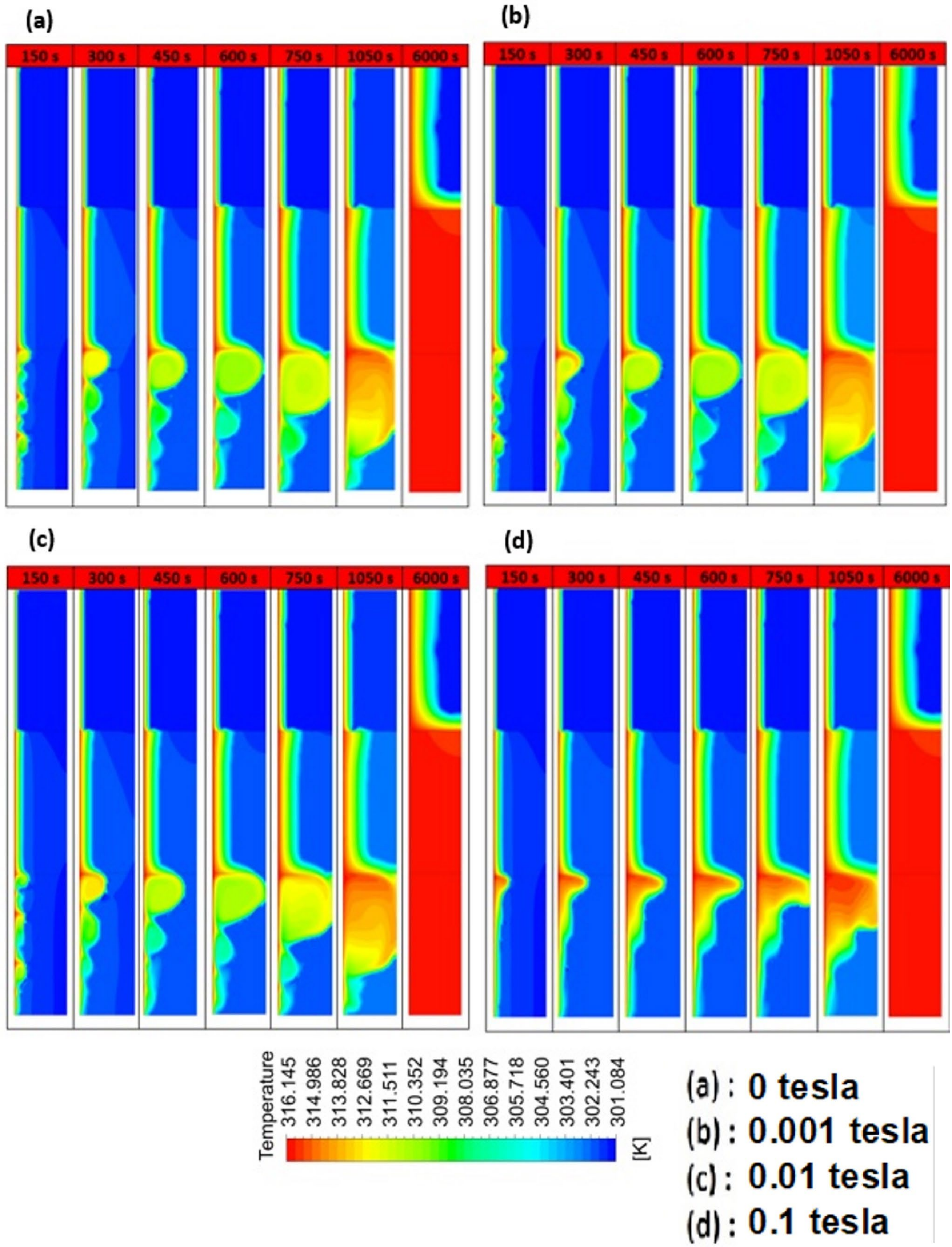
(a)
(b)
(c)
(d)
150 s
300 s
450 s
600 s
750 s
1050 s
6000 s
Temperature
316.145
314.986
313.828
312.669
311.511
310.352
309.194
308.035
306.877
305.718
304.560
303.401
302.243
301.084
[K]
(a) : 0 tesla
(b) : 0.001 tesla
(c) : 0.01 tesla
(d) : 0.1 tesla

Fig. 10 Contour plots of the temperature distributions through the melting progression at a heated wall temperature of 43°C

different conditions such as B_0, show that the current computational model is accurate in predicting the behavior of the thermal system. This verification also re-asserts the reliability of the assay in the examination of numeric tropes within the research, so allowing for further utilization in the exploration and extension of PCM concerns.

In this study, Fig. 4 describes the effect of magnetic flux density on the liquid-to-solid phase change of the material through the analysis of the fluid fraction of the PCM as a function of time. The liquid fraction changes throughout the melting process are shown on the graph, and each curve corresponds to a different strengthening of the magnetized force. A clear trend in the enhancement in the liquid fraction with increasing magnetic flux density is evident suggesting an increase in the melting rate of the PCM. This behaviour can be attributed to the influence of a magnetized force on the thermophysical properties of PCM, particularly thermal conductivity and convection currents. Because of these findings, magnetic flux density is a critical determinant in enhancing phase change in PCMs to boost the functioning of TES systems.

Figure 5 shows the temperature of the PCM as a function of time at different magnetic flux densities. The graph points out very clearly the temperature trends corresponding to the different magnetic field strengths, in as much as it depicts how the spatial average temperatures of the PCM changes throughout the melting development. It is worth mentioning that the upsurge of the magnetic flux density implies an upsurge in average temperature which means that the application of magnetic field helps to intensify thermal energy transfer in PCM. This is expected because of the developed convective currents and effective heat transference as provided by the magnetic increasing the rate of melting.

Average Nusselt number (Nu_{avg}) of the PCM over time for different magnetic flux densities is presented in Fig. 6. From the graph, it is observed that Nu_{avg} rises with the employment of greater magnetic flux densities which according to the investigation suggests that the convection heat transference rate inside the PCM is enhanced during the phase transformation. As it is seen, an increase in the Nusselt number is traced to enhanced thermal characteristics as boosted by the magnetized force indicating heightened fluid motion and heat transfer. The findings therefore confirm the impact of the magnetized flux density on the convection heat transference attributes of the PCMs and indicate that there could be an opportunity to enhance the effectiveness of their use in practical applications through controlling magnetic fields.

The thermal performance of the PCM is illustrated in the average of the total surface heat flux in Fig. 7 at various magnetic flux densities. The graph also shows that the greater the magnetized fluxing density, the greater the heat flux, which implies that the employment of a magnetic field accelerates heat transference at the surface of the PCM. This enhancement can be ascribed to the deed that an increment in the convection currents with the help of a magnetized force improves the thermal contact and heat transference on the surface of the PCM. The outcome analyses suggest that the magnetic flux density is a significant factor for high heat transfer coefficients within TES incorporating PCMs. Figure 8 shows the thermal behaviour of the phase change material (PCM) in the form of average total enthalpy variations concerning the time on the horizontal axis but against different magnetic flux densities on the vertical axis. The curve in Fig. 6 shows that the mean total enthalpy escalates with an increment in magnetized fluxing densities proving the fact that this magnetized force has a quest influence on the heat storage capacity of the PCM. This increase in enthalpy can be ascribed to the better heat transference processes produced by the magnetic field that accelerates the rate of heat-induced phase change in the PCM. As applied to thermal energy storage schemes with PCMs, flux density may well constitute a key factor for maximizing energy storage efficiency when controlled optimally.

As illustrated in Fig. 9, the phase change material (PCM) solid–liquid interfaces during the melting procedure maintain the heated wall temperature at 43°C. This feature is depicted in the visual diagram where the state boundaries are clearly shown as the PCM melts as it is heated by the wall. The figure is concerned with the thermal processes depicted, and how the PCM stores thermal energy as it changes phases. The temperature differences set involving the heated side and the PCM permits the subsequent phase transition hence proving the capability of the material as a TES.

In this investigation, the contour plots depicting the temperature distributions in the PCM throughout the melting process at a heated wall temperature of 43°C are presented in Fig. 10. The contour plots indicate a distinct temperature profile where the warmer regions are closer to the heated wall and in contrast, the cooler regions grow further as we move away from the wall into the PCM. They reflect temperature distribution across the spatial volume of the material during the melting phase when heat is being transmitted from the wall to the PCM and performing phase change from solid-state to liquid. The shapes also exhibit how the PCM manages to store and distribute heat, as well as the formation of thermal layers within the material.

Figure 11 and Table 2 show the outline charts of the velocity field at diverse PCM through the melting progression heated the wall temperature is 43°C. From the velocity field, one can depict the flow patterns obtained while the PCM is

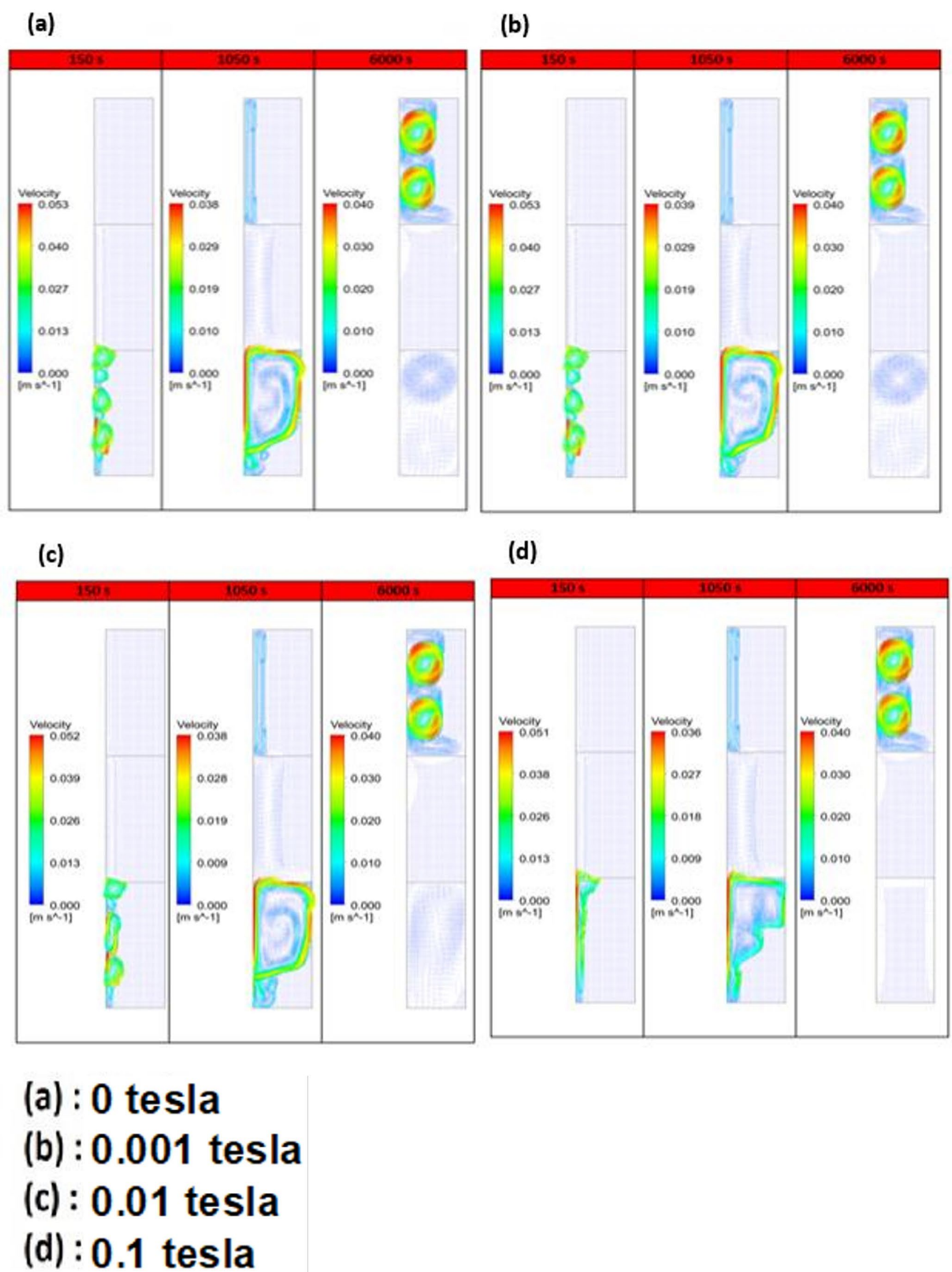
(a)
(b)
(c)
(d)
150 s
1050 s
6000 s
Velocity
[m s^-1]
(a) : 0 tesla
(b) : 0.001 tesla
(c) : 0.01 tesla
(d) : 0.1 tesla

Fig. 11 Contour plots of the Velocity field distributions through the melting progression at a heated wall temperature of 43°C

in the process of changing from the solid phase to the liquid phase, with the convection currents fostered because of the temperature differences between the edge and the core that is heated. These plots suggest that the direction of the fluid motion is towards the heated surface and helps to develop the heat transference and distribution of the molten PCM uniformly. For convection current to upsurge the melting of the PCM, these currents must be present to enable the covering of more area hence enhancing the thermic implementation of the PCM by undertaking time to reduce its thermal mass.

Conclusions

In this examination, the behaviour of phase change materials (PCMs) through the phase change process of melting is the primary focus, with specific reference to the effects of a heated wall at a temperature of 43°C. The current study also emphasizes the importance of understanding the thermal phenomena and fluid mixing on the implementation of thermal energy storing. The subsequent inferences can be drawn:

1. The use of a heated wall enhances the heat transference rates to the PCM than when using a plane wall, thus enhancing the melting development. The temperature distribution illustrates that the PCM stores thermal energy, which is worthy to achieve the maximum storage capacitance of the material.
2. Unlike the phase boundaries for transfer from solid to liquid or liquid to solid, the boundary at the transition between phases of solid and liquid can be highlighted through the contour plots. This transition is important for the performance of PCMs in thermal control applications because it determines how the competence of the material to save and distribute energy is affected.
3. Analysis of the vorticity field introduces patterns of convection currents within the PCM because of the applied temperature gradient across the heated wall. These currents improve the circulation of the material and thus improve the melting of the material as well as minimizing thermal stratification for the best heat exchange.
4. Using metal foam with porosity 0.95 with 5% Al_2O_3 nanoparticle to balance conductivity and fluidity, and applying a uniform magnetic field of $B_0 \approx 0.001T$ near the heated wall to increase the load without increasing complexity or cost, the magnetic field direction was set perpendicular to the flux taking advantage of Lorentz forces.
5. Combining metal foam, which improves conductivity, nanoparticles that enhance thermal properties, and a magnetic field that improves load led to a 53% reduction in overall melting time. It also resulted in a 135% increase in the average Nusselt number compared to pure PCM. This shows that the combined effect is greater than the sum of the individual effects.
6. The system that combines metal foam, nanoparticles, and a magnetic field shows a strong effect. It reduces melting time by about 53% when compared to pure PCM and by around 28% when compared to the non-magnetic composite.
7. Quantitative analysis shows that the magnetic field ($B_0 = 0.001T$) boosts the average Nusselt number by about 34% and increases the surface heat flux by around 72%. This highlights its strong role in improving convective heat transfer in structured PCM composites.

Therefore, this research highlights the role of the thermal and fluid characteristics of PCMs that are necessary for improving the advancement of thermal energy storage systems.

Assumptions, limitations and future work

The basic assumptions and limitations of the current model can be summarized as follows:

- It is assumed that all properties such as viscosity, specific heat, and thermal conductivity are constant for each phase, this slightly simplification maybe affects accuracy in cases where the temperature gradients are large.
- It is taken into consideration that these effects are minimal under the studied configuration and operating conditions of the current study.
- The foam was mixed as a homogeneous porous medium with constant porosity and permeability, neglecting local heterogeneity.
- We also assumed that the magnetic field is constant and uniform, in addition to neglecting all spatially variable or transient magnetic effects.
- Non-slip constraints were applied in the boundary constraints and are valid as a measure of total flow.

These assumptions are based on our reading of similar previous studies using the phase-change materials model and hydromagnetodynamics, which are justified in explaining the prevailing physical phenomena. Future studies may work to mitigate some of these assumptions to further complicate the problem under investigation.

Author contributions A C; S.M; R.B : Conceptualization, Methodology, Software, Formal analysis, Writing – original draft. F.L.R; K.R.E; B.S : Writing–original draft, Data curation, Investigation, Visualization. N.T : Conceptualization, Writing–original draft, Writing–review & editing, Supervision, Resources. I.M; M. K; S.M.R: Writing review & editing; software; and Writing – original draft.

Data availability Manuscript has no associated data.

Declarations

Conflict of interest The authors declare no competing interests.

References

Andersson HI, Bech KH, Dandapat BS (1992) Magnetohydrodynamic flow of a power-law fluid over a stretching sheet. Int J Non-Linear Mech 27:929–936. https://doi.org/10.1016/0020-7462(92)90045-9

Bechiri M, Mansouri K (2016) Analytical study of heat generation effects on melting and solidification of nano-enhanced PCM inside a horizontal cylindrical enclosure. Appl Therm Eng 104:779–790. https://doi.org/10.1016/j.applthermaleng.2016.05.105

Bouzennada T, Mechighel F, Filali A, Kolsi L (2020) Study of the usability of sinusoidal function heat flux based on enthalpy-porosity technique for PCM-related applications. J Therm Anal Calorim 141:1769–1784. https://doi.org/10.1007/s10973-019-09192-7

Chibani A, Dehane A, Merouani S, Bougriou C, Guerraiche D (2022) Melting/solidification of phase change material in a multi-tube heat exchanger in the presence of metal foam: effect of the geometrical configuration of tubes. Energy Storage Saving 1:241–258. https://doi.org/10.1016/j.enss.2022.07.004

Chibani A, Merouani S, Laidoudi H, Dehane A, Bendada L, Lamiri L, Mecheri G, Bougriou C, Gherraf N (2023a) Numerical simulation and analysis of heat transfer and melting rate of nano-enhanced PCM composite embedded in a concentrator photovoltaic system. J Energy Storage 73:109247. https://doi.org/10.1016/j.est.2023.109247

Chibani A, Merouani S, Laidoudi H, Dehane A, Morakchi MR, Bendada L (2023b) Analysis and optimization of concentrator photovoltaic system using a phase change material (RT 35HC) combined with variable metal fins. J Energy Storage 72:108283. https://doi.org/10.1016/j.est.2023.108283

Chibani A, Boucetta C, Merouani S (2024) Enhancing heat transfer and melting rate in large-scale gallium cavity: the impact of buoyancy forces and magnetohydrodynamics. J Magn Magn Mater 592:171780. https://doi.org/10.1016/j.jmmm.2024.171780

Chorin P, Moreau F, Saury D (2018) Heat transfer modification induced by a localized thermal disturbance in a differentially-heated cavity. Int J Therm Sci 125:101–110. https://doi.org/10.1016/j.ijthermalsci.2017.11.018

Çolak E, Oztop HF, Ekici O (2022) Analysis of the gallium melting problem with different heating configurations. J Energy Storage. https://doi.org/10.1016/j.est.2022.104651

Dahmani A, Muñoz-Cámara J, Laouedj S, Solano JP (2022) Heat transfer enhancement of ferrofluid flow in a solar absorber tube under non-uniform magnetic field created by a periodic current-carrying wire. Sustain Energy Technol Assess 52:101996. https://doi.org/10.1016/j.seta.2022.101996

Feng S, Shi M, Li Y, Lu TJ (2015) Pore-scale and volume-averaged numerical simulations of melting phase change heat transfer in finned metal foam. Int J Heat Mass Transf 90:838–847. https://doi.org/10.1016/j.ijheatmasstransfer.2015.06.088

Ghalambaz M, Doostani A, Izadpanahi E, Chamkha AJ (2017) Phase-change heat transfer in a cavity heated from below: the effect of utilizing single or hybrid nanoparticles as additives. J Taiwan Inst Chem Eng 72:104–115. https://doi.org/10.1016/j.jtice.2017.01.010

Golbaghi Masouleh SS, Nikian M, Ghazi M (2022) Analytical study on core flow in a novel scheme of cascade heat exchanger intensified with open foam partially filled in an annulus. Int J Therm Sci 177:107568. https://doi.org/10.1016/j.ijthermalsci.2022.107568

Gorzin M, Hosseini MJ, Rahimi M, Bahrampoury R (2019) Nano-enhancement of phase change material in a shell and multi-PCM-tube heat exchanger. J Energy Storage 22:88–97. https://doi.org/10.1016/j.est.2018.12.023

Hashemi-Tilehnoee M, Dogonchi AS, Seyyedi SM, Chamkha AJ, Ganji DD (2020) Magnetohydrodynamic natural convection and entropy generation analyses inside a nanofluid-filled incinerator-shaped porous cavity with wavy heater block. J Therm Anal Calorim 141:2033–2045. https://doi.org/10.1007/s10973-019-09220-6

Hosseinizadeh SF, Tan FL, Moosania SM (2011) Experimental and numerical studies on performance of PCM-based heat sink with different configurations of internal fins. Appl Therm Eng 31:3827–3838. https://doi.org/10.1016/j.applthermaleng.2011.07.031

Hu X, Patnaik SS (2014) Modeling phase change material in micro-foam under constant temperature condition. Int J Heat Mass Transf 68:677–682. https://doi.org/10.1016/j.ijheatmasstransfer.2013.09.054

Huang Z, Zhang W, Xi G (2015) Natural convection heat transfer in a cubic cavity submitted to time-periodic sidewall temperature. Numer Heat Transf Part A Appl 67:13–32. https://doi.org/10.1080/10407782.2013.798550

Ji C, Qin Z, Low Z, Dubey S, Choo FH, Duan F (2018) Non-uniform heat transfer suppression to enhance PCM melting by angled fins. Appl Therm Eng 129:269–279. https://doi.org/10.1016/j.applthermaleng.2017.10.030

Kang K-G, Ryou H-S (2004) Computation of solidification and melting using the PISO algorithm. Numer Heat Transf B Fundam 46:179–194. https://doi.org/10.1080/10407790490438563

Kant K, Anand A, Shukla A, Sharma A (2020) Heat transfer study of building integrated photovoltaic (BIPV) with nano-enhanced phase change materials. J Energy Storage 30:101563. https://doi.org/10.1016/j.est.2020.101563

Keshteli AN, Sheikholeslami M (2020) Influence of Al2O3 nanoparticle and Y-shaped fins on melting and solidification of paraffin. J Mol Liq. https://doi.org/10.1016/j.molliq.2020.113798

Khademi A, Shank K, Mehrjardi SAA, Tiari S, Sorrentino G, Said Z, Chamkha AJ, Ushak S (2022) A brief review on different hybrid methods of enhancement within latent heat storage systems. J Energy Storage 54:105362. https://doi.org/10.1016/j.est.2022.105362

Khan Z, Khan ZA, Sewell P (2019) Heat transfer evaluation of metal oxides based nano-PCMs for latent heat storage system application. Int J Heat Mass Transf 144:118619. https://doi.org/10.1016/j.ijheatmasstransfer.2019.118619

Khan MI, Waqas H, Farooq U, Khan SU, Chu Y-M, Kadry S (2021) Assessment of bioconvection in magnetized Sutterby nanofluid configured by a rotating disk: a numerical approach. Mod Phys Lett B 35:2150202. https://doi.org/10.1142/S021798492150202X

Kıyak B, Öztop HF, Aksoy İG (2024) Experimental and numerical investigation on melting of phase change material in a disc-shaped container via hot air jet impinging. Appl Therm Eng 236:121761. https://doi.org/10.1016/j.applthermaleng.2023.121761

Kok B (2020) Examining effects of special heat transfer fins designed for the melting process of PCM and Nano-PCM. Appl Therm Eng. https://doi.org/10.1016/j.applthermaleng.2020.114989

Kumar P, Topin F (2014) Micro-structural impact of different strut shapes and porosity on hydraulic properties of Kelvin-like metal foams. Transp Porous Media 105:57–81. https://doi.org/10.1007/s11242-014-0358-8

Leong KY, Hasbi S, Gurunathan BA (2021) State of art review on the solidification and melting characteristics of phase change material in triplex-tube thermal energy storage. J Energy Storage 41:102932. https://doi.org/10.1016/j.est.2021.102932

Li Z, Shahsavar A, Al-Rashed AAAA, Talebizadehsardari P (2020) Effect of porous medium and nanoparticles presences in a counter-current triple-tube composite porous/nano-PCM system. Appl Therm Eng 167:114777. https://doi.org/10.1016/j.applthermaleng.2019.114777

Lu W, Zhao CY, Tassou SA (2006) Thermal analysis on metal-foam filled heat exchangers. Part I: metal-foam filled pipes. Int J Heat Mass Transf 49:2751–2761. https://doi.org/10.1016/j.ijheatmasstransfer.2005.12.012

Mesalhy O, Lafdi K, Elgafy A, Bowman K (2005) Numerical study for enhancing the thermal conductivity of phase change material (PCM) storage using high thermal conductivity porous matrix. Energy Convers Manag 46:847–867. https://doi.org/10.1016/j.enconman.2004.06.010

Moghadassi A, Ghomi E, Parvizian F (2015) A numerical study of water based Al_2O_3 and Al_2O_3–Cu hybrid nanofluid effect on forced convective heat transfer. Int J Therm Sci 92:50–57. https://doi.org/10.1016/j.ijthermalsci.2015.01.025

Nóbrega CRES, Ismail KAR, Lino FAM (2020) Solidification around axial finned tube submersed in PCM: modeling and experiments. J Energy Storage. https://doi.org/10.1016/j.est.2020.101438

Öztop HF, Gür M, Selimefendigil F, Coşanay H (2024) Impacts of inclined plate on melting time for phase change material filled blocks: experimental and numerical analysis. Therm Sci Eng Prog 48:102427. https://doi.org/10.1016/j.tsep.2024.102427

Prasad KV, Mebarek-Oudina F, Vaidya H, Choudhari R, Karanth S, Tripathi D (2024) Tangent hyperbolic MHD nanoliquids on non-isothermal stretched sheets: analyzing the impact of transport parameters, variable fluid properties and convective boundary conditions. Results Phys 66:108008. https://doi.org/10.1016/j.rinp.2024.108008

Rostami S, Afrand M, Shahsavar A, Sheikholeslami M, Kalbasi R, Aghakhani S, Shadloo MS, Oztop HF (2020) A review of melting and freezing processes of PCM/nano-PCM and their application in energy storage. Energy 211:118698. https://doi.org/10.1016/j.energy.2020.118698

Saha SK (2020) Magnetohydrodynamic buoyancy driven Al2O3-water nanofluid flow in a differentially heated trapezoidal enclosure with a cylindrical barrier. Int Commun Heat Mass Transf 114:104593. https://doi.org/10.1016/j.icheatmasstransfer.2020.104593

Seeniraj RV, Lakshmi Narasimhan N (2008) Performance enhancement of a solar dynamic LHTS module having both fins and multiple PCMs. Sol Energy 82:535–542. https://doi.org/10.1016/j.solener.2007.11.001

Selimefendigil F, Öztop HF, Abu-Hamdeh N (2022) Optimization of phase change process in a sinusoidal-wavy conductive walled cylinder with encapsulated-phase change material during magnetohydrodynamic nanofluid convection. J Energy Storage 55:105512. https://doi.org/10.1016/j.est.2022.105512

Shakiba A, Vahedi K (2016) Numerical analysis of magnetic field effects on hydro-thermal behavior of a magnetic nanofluid in a double pipe heat exchanger. J Magn Magn Mater 402:131–142. https://doi.org/10.1016/j.jmmm.2015.11.039

Shatikian V, Ziskind G, Letan R (2005a) Numerical investigation of a PCM-based heat sink with internal fins. Int J Heat Mass Transf 48:3689–3706. https://doi.org/10.1016/j.ijheatmasstransfer.2004.10.042

V. Shatikian, G. Ziskind, R. Letan (2005b) Transient performance of a finned PCM heat sink, pp. 137–142. https://doi.org/10.1115/IPACK2005-73113

Tadrist L, Miscevic M, Rahli O, Topin F (2004) About the use of fibrous materials in compact heat exchangers. Exp Therm Fluid Sci 28:193–199. https://doi.org/10.1016/S0894-1777(03)00039-6

Tian Y, Zhao CY (2011) A numerical investigation of heat transfer in phase change materials (PCMs) embedded in porous metals. Energy 36:5539–5546. https://doi.org/10.1016/j.energy.2011.07.019

Vafai K, Tien CL (1981) Boundary and inertia effects on flow and heat transfer in porous media. Int J Heat Mass Transf 24:195–203. https://doi.org/10.1016/0017-9310(81)90027-2

Vajjha RS, Das DK, Namburu PK (2010) Numerical study of fluid dynamic and heat transfer performance of Al2O3 and CuO nanofluids in the flat tubes of a radiator. Int J Heat Fluid Flow 31:613–621. https://doi.org/10.1016/j.ijheatfluidflow.2010.02.016

Voller VR, Prakash C (1987) A fixed grid numerical modelling methodology for convection-diffusion mushy region phase-change problems. Int J Heat Mass Transf 30:1709–1719. https://doi.org/10.1016/0017-9310(87)90317-6

Wang L, Kan A, Yu W (2022) Melting behavior and heat transfer performance in a modified PCM-filled enclosure with fins under hypergravity conditions. Int Commun Heat Mass Transf 138:106415. https://doi.org/10.1016/j.icheatmasstransfer.2022.106415

Zennouhi H, Benomar W, Kousksou T, Msaad AA, Allouhi A, Mahdaoui M, El Rhafiki T (2017) Effect of inclination angle on the melting process of phase change material. Case Stud Therm Eng 9:47–54. https://doi.org/10.1016/j.csite.2016.11.004